Novel Synthesis Method of CO-Tolerant PtRu−MoO_x Nanoparticles: Structural Characteristics and Performance for Methanol Electrooxidation

M. V. Martínez-Huerta,*,† J. L. Rodríguez,† N. Tsiouvaras,‡ M. A. Peña,‡ J. L. G. Fierro,‡ and E. Pastor†

Departamento de Química Física, Universidad de La Laguna, Astrofísico Francisco Sánchez s/n, 38071, La Laguna, Tenerife, Spain and Instituto de Catálisis y Petroleoquímica, CSIC, Marie Curie 2, Cantoblanco, 28049 Madrid, Spain

Received October 24, 2007. Revised Manuscript Received April 11, 2008. Accepted April 14, 2008

Carbon-supported PtRu−MoO_x nanoparticles with significant CO tolerance were prepared by a new two-step procedure: in the first step, molybdenum oxide was deposited on a carbon substrate (MoO_x/C) by impregnation, and in the second one, Pt and Ru were incorporated following a colloidal method with $NaHSO_3$. The composition, particle size, and crystallinity of the catalysts were determined by X-ray analytical methods (X-ray diffraction (XRD), X-ray photoelectron spectroscopy (XPS), and total-reflection X-ray fluorescence (TXRF)), transmission electron microscopy (TEM), and thermogravimetry (TG). Conventional electrochemical techniques such as cyclic voltammetry (CV) and chronoamperometry were applied in combination with spectroscopic methods adapted to the electrochemical systems for in situ studies, such as Fourier transform infrared spectroscopy (FTIRS) and differential electrochemical mass spectrometry (DEMS). The results of this work are highly encouraging, as it is proved that a reduction of the amount of precious metals Pt and Ru is possible in parallel with a significant increase of CO tolerance in comparison with commercial catalysts.

Introduction

The development of metal nanoparticles with a high tolerance toward CO oxidation is one of the main research tasks in the field of polymer electrolyte membrane fuel cells (PEMFC).[1,2] These PEMFC systems have emerged as promising electrical supply devices for transportation, involving both stationary and portable applications, although they are only satisfactory when fed with pure hydrogen fuel. However, the production, storage, and refueling infrastructures of pure hydrogen pose significant problems. The hydrogen-rich synthetic gas obtained from steam reforming of hydrocarbons or partial oxidation of alcohols is a practical fuel for PEMFC.[3,4] A much simpler approach is the direct methanol fuel cell (DMFC) in which the reforming step is eliminated, thus making it more suitable for portable applications. Although DMFC is an attractive approach, it requires more than 10 times the amount of Pt catalyst than reforming gas fed PEMFC.[5,6] In both cases, the carbon monoxide (CO) formed as byproduct strongly adsorbs on the catalytic platinum surface at the anode, drastically blocking the hydrogen oxidation reaction. It is essential, therefore, to develop much more active electrocatalysts, mainly Pt-based ones, at a lower cost.[7,8]

The PtRu nanoparticle catalysts have recorded the best performance among the binary catalysts examined. Considerable effort has been done to clarify the nature of Ru promotion on Pt in the methanol and CO electrooxidation,[9–11] and numerous works have been devoted to the synthesis of this kind of catalysts.[2,12–15] Oxidation of adsorbed CO is postulated to be the rate-determining step, and Ru is widely accepted as a promoter for CO oxidation, commonly explained on the basis of the bifunctional mechanism[16] or the "ligand effect"[17] or a combination of the two. The bifunctional mechanism assumes that Ru promotes oxidation

* To whom correspondence should be addressed. E-mail: mvmartin@ull.es.
† Universidad de La Laguna.
‡ Instituto de Catálisis y Petroleoquímica.

(1) Watanabe, M. In *Handbook of Fuel Cells. Fundamental Technology and Applications*; Vielstich, W., Gasteiger, H. A., Lamm, A., Eds.; Wiley: Chichester, 2003; Vol. 2, p 408.
(2) Wee, J. H.; Lee, K. Y. *J. Power Sources* **2006**, *157*, 128.
(3) Antolini, E. *J. Appl. Electrochem.* **2004**, *34*, 563.
(4) Jacobson, M. Z.; Colella, W. G.; Golden, D. M. *Science* **2005**, *308*, 1901.
(5) Liu, H.; Song, C.; Zhang, L.; Zhang, J.; Wang, H.; Wilkinson, D. P. *J. Power Sources* **2006**, *155*, 95.
(6) Dillon, R.; Srinivasan, S.; Arico, A. S.; Antonucci, V. *J. Power Sources* **2004**, *127*, 112.
(7) Aricò, A. S.; Srinivasan, R.; Antonucci, V. *Fuel Cells* **2001**, *1*, 133.
(8) Iwasita, T. In *Handbook of Fuel Cells. Fundamental Technology and Applications*; Vielstich, W., Gasteiger, H. A., Lamm, A., Eds.; Wiley: Chichester, 2003; Vol. 2, p 603.
(9) Hamnett, A. *Catal. Today* **1997**, *38*, 445.
(10) Tong, Y. Y.; Kim, H. S.; Babu, P. K.; Waszczuk, P.; Wieckowski, A.; Oldfield, E. *J. Am. Chem. Soc.* **2002**, *124*, 468.
(11) Babu, P. K.; Kim, H. S.; Kuk, S. T.; Chung, J. H.; Oldfield, E.; Wieckowski, A. *J. Phys. Chem. B* **2005**, *109*, 17192.
(12) Antolini, E. *Mater. Chem. Phys.* **2003**, *78*, 563.
(13) Bönnemann, H.; Brijoux, W.; Brinkmann, R.; Fretzen, R.; Joussen, T.; Köppler, R.; Korall, B.; Neiteler, P.; Richter, J. *J. Mol. Catal. A: Chem.* **1994**, *86*, 129.
(14) Liu, Z.; Ada, E. T.; Shamsuzzoha, M.; Thompson, G. B.; Nikles, D. E. *Chem. Mater.* **2006**, *18*, 4946.
(15) Watanabe, M.; Uchida, M.; Motoo, S. *J. Electroanal. Chem.* **1987**, *229*, 395.
(16) Watanabe, M.; Motoo, S. *J. Electroanal. Chem.* **1975**, *60*, 267.
(17) Frelink, T.; Visscher, W.; van Veen, J. A. R. *Surf. Sci.* **1995**, *335*, 353.

10.1021/cm703047p CCC: $40.75
Published on Web 06/04/2008

of the strongly bound CO on Pt by supplying an oxygen source ($Ru-OH_{ad}$). According to the ligand effect, the energy level of the catalyst is changed so that the binding strength of adsorbed CO is weakened, thereby reducing the oxidation overpotential. However, much greater durability and lower cost of the anode catalysts are required for practical PEMFC applications. Some of the main research tasks in the field of fuel cells currently involve development of materials with smaller amounts of noble metal and high tolerance toward CO oxidation.

Addition of Mo on Pt[18–27] and PtRu[28–39] catalysts has therefore attracted major attention in recent years. The CO-tolerance mechanism of PtMo catalysts has been discussed in the literature.[40,41] Studies of CO oxidation on polycrystalline PtMo alloys indicate that the conventional bifunctional mechanism is responsible for the CO tolerance of these materials. Water-induced oxide formation has therefore been attributed to Mo,[42] which shows high water dissociation capability. Additionally, formation of a molybdenum hydrogen bronze H_yMoO_x due to the proton spillover from Pt sites to Mo has been suggested as a possible explanation for enhanced CO tolerance.[43] This effect was previously studied by Tseung et al. in Pt/WO_3 systems,[44,45] in which the transfer of protons, produced on the platinum surface during electrooxidation of methanol, to the tungsten oxide generate a hydrogen tungsten bronze species (H_xWO_3). These authors also considered this effect as responsible to maintain clean platinum surface, thus enhancing the electrooxidation current density. Thus, the CO oxidation mechanism on ternary PtRuMo/C systems has been explained by hydrogen and CO spillover effects and the bifunctional mechanism.[37]

The role of molybdenum has yet to be fully determined. The molybdenum−oxygen system contains five distinct phases (Magneli phases) with compositions between MoO_2 and MoO_3.[46] These mixed-valence oxides of molybdenum, MoO_x, have a rutile-type structure with a short metal−metal bond distance along the direction of edge sharing, which accounts for the high electronic conductivity of these materials. Besides the metallic conductivity, MoO_x are relatively stable in acid solution and have specific catalytic reactivity toward reduction of O_2.[46] The distribution of Mo oxide species on supported Mo-based systems is influenced by the catalyst preparation method, such as the nature of the Mo precursor, the support, and the drying or calcination conditions.[47–51]

Various synthesis methods for the preparation of carbon-supported PtRuMo nanoparticles have been described in the literature:[52,53] (i) adsorption of platinum and metal colloids onto the carbon surface and (ii) impregnation of carbon support with Pt and M precursor solution. (i) The colloid method commonly used to prepare PtRuMo nanoparticles is the Bonnemann method.[54] Götz and Wendt[39] found that this method provides an excellent tool for synthesizing polymetallic PtRuMe (Me = W, Mo, and Sn) nanoparticles deposited on a carbon substrate, being more effective than the impregnation method. They tested catalysts with a molar ratio of 1:1:1 for Pt/Ru/Me for oxidation of methanol and H_2/CO in fuel cell operation and observed that the system Pt/Ru/W was superior to the other systems tested. (ii) Papageorgopoulos et al.[38] prepared 20 wt % PtRuMe (Me = Mo, Nb) metal particles on a carbon carrier with a molar ratio of 9:9:2 for Pt/Ru/Me by one-step deposition of the metals from their corresponding salts with formaldehyde as the reducing agent. They did not find a significant difference for CO electrooxidation at the lower potential limit, compared to the PtRu/C system. However, fuel cell tests revealed that while all the prepared catalysts exhibited enhanced performance for PEMFC compared to Pt/C, only addition of a relatively small amount of Mo to PtRu results in an electrocatalyst with a higher activity. Recently, Hou et al.[37] prepared a $PtRu-H_xMeO_3/C$ (Me = Mo, W) system by a composite support method. First, they prepared a composite

(18) Urian, R. C.; Gullá, A. F.; Mukerjee, S. *J. Electroanal. Chem.* **2003**, *554*, 307.
(19) Ioroi, T.; Yasuda, K.; Siroma, Z.; Fujiwara, N.; Miyazaki, Y. *J. Electrochem. Soc.* **2003**, *150*, A1225.
(20) Mukerjee, S.; Urian, R. C.; Lee, S. J.; Ticianelli, E. A.; McBreen, J. *J. Electrochem. Soc.* **2004**, *151*, A1094.
(21) Santiago, E. I.; Batista, M. S.; Assaf, E. M.; Ticianelli, E. A. *J. Electrochem. Soc.* **2004**, *151*, A944.
(22) Mylswamy, S.; Wang, C. Y.; Liu, R. S.; Lee, J. F.; Tang, M. J.; Lee, J. J.; Weng, B. J. *Chem. Phys. Lett.* **2005**, *412*, 444.
(23) Ordonez, L. C.; Roquero, P.; Sebastian, P. J.; Ramirez, J. *Catal. Today* **2005**, *107−108*, 46.
(24) Lebedeva, N. P.; Janssen, G. J. M. *Electrochim. Acta* **2005**, *51*, 29.
(25) Ioroi, T.; Akita, T.; Yamazaki, S. I.; Siroma, Z.; Fujiwara, N.; Yasuda, K. *Electrochim. Acta* **2006**, *52*, 491.
(26) Grgur, B. N.; Markovic, N. M.; Ross, P. N. *J. Electrochem. Soc.* **1999**, *146*, 1613.
(27) Wang, Y.; Rosim Fachini, E.; Cruz, G.; Zhu, Y.; Ishikawa, Y.; Colucci, J. A.; Cabrera, C. R. *J. Electrochem. Soc.* **2001**, *148*, C222.
(28) Lasch, K.; Jörissen, L.; Garche, J. *J. Power Sources* **1999**, *84*, 225.
(29) Lima, A.; Coutanceau, C.; Leger, J. M.; Lamy, C. *J. Appl. Electrochem.* **2001**, *31*, 379.
(30) Lima, A.; Hahn, F.; Léger, J.-M. *Russ. J. Electrochem.* **2004**, *40*, 326.
(31) Jusys, Z.; Schmidt, T. J.; Dubau, L.; Lasch, K.; Jörissen, L.; Garche, J.; Behm, R. J. *J. Power Sources* **2002**, *105*, 297.
(32) Franco, E. G.; Neto, A. O.; Linardi, M.; Arico, E. *J. Braz. Chem. Soc.* **2002**, *13*, 516.
(33) Oliveira Neto, A.; Franco, E. G.; Arico, E.; Linardi, M.; Gonzalez, E. R. *J. Eur. Ceram. Soc.* **2003**, *23*, 2987.
(34) Zhang, X.; Zhang, F.; Chan, K. Y. *J. Mater. Sci.* **2004**, *39*, 5845.
(35) Song, C. J.; Khanfar, M.; Pickup, P. G. *J. Appl. Electrochem.* **2006**, *36*, 339.
(36) Benker, N.; Roth, C.; Mazurek, M.; Fuess, H. *J. New Mater., Electrochem. Syst.* **2006**, *9*, 121.
(37) Hou, Z.; Yi, B.; Yu, H.; Lin, Z.; Zhang, H. *J. Power Sources* **2003**, *123*, 116.
(38) Papageorgopoulos, D. C.; Keijzer, M.; de Bruijn, F. A. *Electrochim. Acta* **2002**, *48*, 197.
(39) Götz, M.; Wendt, H. *Electrochim. Acta* **1998**, *43*, 3637.
(40) Grgur, B. N.; Zhuang, G.; Markovic, N. M.; Ross, J. P. N. *J. Phys. Chem. B* **1997**, *101*, 3910.
(41) Grgur, B. N.; Markovic, N. M.; Ross, P. N., Jr. *J. Phys. Chem. B* **1998**, *102*, 2494.
(42) Anderson, A. B.; Grantscharova, E.; Seong, S. *J. Electrochem. Soc.* **1996**, *143*, 2075.
(43) Zhang, H.; Wang, Y.; Rosim Fachini, E.; Cabrera, C. R. *Electrochem. Solid State* **1999**, *2*, 437.
(44) Hobbs, B. S.; Tseung, A. C. C. *Nature* **1969**, *222*, 556.
(45) Tseung, A. C. C.; Chen, K. Y. *Catal. Today* **1997**, *38*, 439.
(46) Horkans, J.; Shafer, M. W. *J. Electrochem. Soc.* **1977**, *124*, 1196.
(47) Chary, K. V. R.; Reddy, K. R.; Kishan, G.; Niemantsverdriet, J. W.; Mestl, G. *J. Catal.* **2004**, *226*, 283.
(48) Haber, J.; Lalik, E. *Catal. Today* **1997**, *33*, 119.
(49) Feng, L.; Li, X.; Dadyburjor, D. B.; Kugler, E. L. *J. Catal.* **2000**, *190*, 1.
(50) Rondon, S.; Wilkinson, W. R.; Proctor, A.; Houalla, M.; Hercules, D. M. *J. Phys. Chem.* **1995**, *99*, 16709.
(51) Rajagopal, S.; Marini, H. J.; Marzari, J. A.; Miranda, R. *J. Catal.* **1994**, *147*, 417.
(52) Antolini, E. *Appl. Catal. B: Environ.* **2007**, *74*, 324.
(53) Antolini, E. *Appl. Catal. B: Environ.* **2007**, *74*, 337.
(54) Bönnemann, H.; Brijoux, W.; Brinkmann, R.; Dinjus, E.; Joussen, T.; Korall, B. *Angew. Chem., Int. Ed.* **1991**, *30*, 1312.

carrier with H_xMeO_3 colloid, and subsequently, Pt and Ru metals were added by impregnation using formaldehyde as the reducing agent. Hydrogen and CO spillover effects are believed to occur on transition-metal oxides, leading to a delay in CO poison polarization in PEMFC anode.

In the present work, PtRu−MoO_x nanoparticles deposited on a carbon substrate were prepared following a new two-step procedure, whose main innovation is incorporation of Pt and Ru on a MoO_x/C system, following the colloidal method developed by Watanabe at al.[15] Three different catalysts, denoted PRM1, PRM2, and PRM3, were obtained. The structure and chemical composition of the nanoparticles have been widely characterized. Spectroscopic methods adapted to the electrochemical systems for in situ studies, such as Fourier transform infrared spectroscopy (FTIRS) and differential electrochemical mass spectrometry (DEMS), were used to evaluate the CO tolerance of these systems.

Experimental Section

Synthesis of Nanoparticles. The first step in the synthesis consists of the preparation of three MoO_x/C systems: MoO_x/C(1), MoO_x/C(2), and MoO_x/C(3). Hydrous molybdenum oxide deposited on Vulcan XC-72R (Cabot) to obtain MoO_x/C(1) and MoO_x/C(2) was prepared by the deposition−precipitation method.[55] A 4 g amount of Vulcan XC-72R was dispersed in 100 mL of MeOH under vigorous stirring. The appropriate amount of molybdenum pentachloride ($MoCl_5$, Aldrich) was dissolved in deionized water (>18 MΩ cm) to obtain a 100 mM Mo solution, which was then added to the carbon dispersed solution (5 wt % nominal metal content) and kept under vigorous stirring. Another 50 mL of MeOH was added to the molybdenum−carbon suspension to maintain a higher dispersion of the carbon substrate in the suspension. Five equivalents of tetramethylammonium hydroxide solution were then added dropwise to precipitate the hydrous molybdenum oxide (MoO_xH_y) on the carbon particles. After 1 h aging under stirring, the MoO_xH_y/C solid was recovered by filtration and dried at 110 °C for 17 h to obtain MoO_x/C(1). One aliquot of MoO_x/C(1) was then treated with aqueous H_2O_2 solution (10 v/v %) at room temperature for 48 h under stirring and dried at 110 °C for 24 h. This sample is referred to hereafter as MoO_x/C(2). Finally, molybdenum oxide (MoO_3, Aldrich) deposited on Vulcan XC 72R was prepared by the impregnation method with H_2O_2. A 4 g amount of carbon black was oxidized with aqueous H_2O_2 (30 v/v %) and stirred for 30 min, whereupon an aqueous solution (0.3 M) of MoO_3 (20 wt. % nominal metal content) was added to the mixture. The solution was then stirred for 48 h at room temperature and dried at 110 °C for 24 h to obtain MoO_x/C(3).

In a second step, platinum and ruthenium were loaded on the MoO_x/C(1), MoO_x/C(2), and MoO_x/C(3) samples according to the colloidal methodology.[15] The reaction was performed in water with aqueous solutions of reactants. The appropriate concentration of H_2PtCl_6 was reduced by adding a solution of $Na_2S_2O_5$ ($NaHSO_3$) to obtain a colorless soluble intermediate of platinum, which was then oxidized with H_2O_2 (30%, v/v). During addition the pH of the solution was adjusted to ca. 5 by adding Na_2CO_3. The appropriate amount of $RuCl_3$ solution was then added dropwise under continuous stirring while keeping the pH close to ca. 5. The required amount of carbon black was added to the colloidal solution under constant stirring. Hydrogen gas was bubbled through this admixture for 2 h, and the suspension was allowed to settle, filtered, washed with hot water, and then dried in an air oven at 110 °C for 15 h. Three catalysts were developed: PtRu(1:1)/MoO_x/C(1) (labeled PRM1), PtRu(1:1)/MoO_x/C(2) (labeled PRM2), and PtRu(1:1)/MoO_x/C(3) (labeled PRM3). The nominal metal (Pt + Ru + Mo) content on carbon was 30 wt %. Commercially available electrocatalysts containing 30 wt % PtRu (1:1)/Carbon (Johnson-Matthey) (labeled PtRu/C (JM)) were used for comparison. Solutions were prepared using Millipore-MiliQ water and analytical-grade reagents.

Structural and Surface Characterization Methods. Thermogravimetric analysis (TGA) under controlled atmosphere was carried out on a Mettler Toledo TGA/SDTA851e using 200 cm^3 min^{-1} of N_2 as carrier gas, 20 cm^3 min^{-1} of oxygen as reactive gas, and a heating rate of 10 °C min^{-1}. Inductively coupled plasma-atomic emission spectroscopy (ICP-AES) was used to analyze the molybdenum/carbon samples on a Perkin-Elmer Optima 3300 DV device. Total-reflection X-ray fluorescence (TXRF) was performed on a Seifert EXTRA-II spectrometer equipped with two X-ray fine focus lines, Mo and W anodes and a Si(Li) detector with an active area of 80 mm^2 and a resolution of 157 eV at 5.9 keV (Mn Kα). The Pt/Ru atomic ratio was determined using Pt*L*α and Ru*L*α emission lines in the XRF spectra after proper calibration with standard samples.

Metal phases and crystalline particle size have been determined using X-ray diffraction (XRD) measurements. X-ray diffraction powder patterns were obtained on a Seifert 3000P X-ray diffractometer using a Cu Kα source. The diffraction profiles of the samples were recorded within Bragg's angles ranging from 15° to 90° at a scanning rate of 0.04°/s. Particle size and morphology, as well as PtRu dispersion of the samples, were evaluated from the transmission electron microscopy (TEM) images obtained in a JEOL 2000FX microscope operated with an accelerating voltage of 200 kV. The standard procedure involved dispersing 10 mg of the sample in acetone in an ultrasonic bath for 15 min. The sample was then placed in a Cu carbon grid where the liquid phase was evaporated.

Photoelectron spectra (XPS) were obtained with a VG Escalab 200R spectrometer equipped with a hemispherical electron analyzer (pass energy of 50 eV) and a Mg Kα ($h\nu$ = 1253.6 eV, 1 eV = 1.602×10^{-19} J) X-ray source, powered at 120 W. The kinetic energies of photoelectrons were measured using a hemispherical electron analyzer working in the constant pass energy mode. The background pressure in the analysis chamber was kept below 2×10^{-8} mbar during data acquisition. The XPS data signals were taken in increments of 0.1 eV with dwell times of 50 ms. Binding energies were calibrated relative to the C 1s peak at 284.6 eV. High-resolution spectral envelopes were obtained by curve fitting synthetic peak components using the software XPS peak. The raw data were used with no preliminary smoothing. Symmetric Gaussian−Lorentzian product functions were used to approximate the line shapes of the fitting components.

The H_2 temperature-programmed reduction (H_2-TPR) experiments were run in a Micromeritics equipment model TPR/TPD-2900 fitted with a TCD detector. Samples of ca. 20 mg each were used. The TPR experiments were run in a 10% H_2/Ar stream with a heating rate of 10 °C/min and 80 cm^3/min flow rate.

Electrochemical Methods. All solutions were prepared from Millipore Milli-Q* water and analytical-grade reagents. The electrolytic solutions employed were 0.5 M H_2SO_4 (98% Merck p.a.) for CO electrooxidation experiments and 2 M CH_3OH (99.98% Scharlau) in 0.5 M H_2SO_4. Freshly prepared solutions were purged with Ar (99.998% Air−Liquide). All experiments were carried out in electrochemical cells using a three-electrode assembly. The working electrodes were glassy carbon electrodes for chronoamper-

(55) Ioroi, T.; Fujiwara, N.; Siroma, Z.; Yasuda, K.; Miyazaki, Y. *Electrochem. Commun.* **2002**, *4*, 442.

Table 1. Physicochemical Parameters of the Samples Based on Analysis of TXRF, ICP, TGA, XRD, and TEM

catalyst	Pt/Ru/Mo ratio by TXRF	Pt + RuO_2 + MoO_3 wt % by TGA	metal loading[a] (wt %) Pt	Ru	Mo	particle size (nm) by XRD	particle size (nm) by TEM	surface metal weight[c] (%) Pt/Ru/Mo/S
MoO_x/C(1)		4.9	0	0	3.3 (3.9[b])			0/0/6/0
MoO_x/C(2)		4.9	0	0	3.3 (3.6[b])			0/0/6/0
MoO_x/C(3)		26	0	0	17 (17.3[b])			0/0/12/0
PRM1	1/1.1/0.4	29	14	8	2.7	3.8	3.2	17/12/3.2/2.6
PRM2	1/1.3/0.2	27	13	9	1.4	4	3.7	17/10/1.6/2.2
PRM3	1/0.6/1.5	36	9	5	12	2.7	3.3	15/12/19/0.9
PtRu/C (JM)	1/1/0	34	20	10	0	2.5		23/9/0/0

[a] Values calculated by TXRF and TGA analysis. [b] ICP analysis. [c] XPS analysis.

ometry (CA) (3.0 mm diameter) and for DEMS (7.0 mm diameter), and an Au disk for FTIRS (10 mm diameter). The counter electrode was a platinum wire for methanol electrooxidation and glassy carbon for DEMS and FTIRS. For methanol current−time curves, Hg/Hg_2SO_4 was used as the reference electrode, although data in the paper are referenced to the reversible hydrogen electrode (RHE). Similarly, a reversible hydrogen electrode (RHE) in the supporting electrolyte was employed as the reference electrode for DEMS and FTIRS. In all experiments, the working electrode was activated in the supporting electrolyte solution by potential cycling between 0 and 0.80 V and one cycle between 0.0 and 1.15 V. The working electrode was prepared according to a modified method developed by Schmidt et al.[56] The standard procedure involved dispersing 4 mg of the electrocatalysts in water (1 mL) and Nafion (30 μL) in an ultrasonic bath for 45 min. Appropriate amounts of the ink were deposited onto the electrode and dried in an Ar flow for 30 min.

Differential electrochemical mass spectrometry (DEMS) experiments were carried out in a 2 cm^3 plexiglass flow cell directly attached to the vacuum chamber of the mass spectrometer (Balzers QMG112) with a Faraday cup detector. The experimental setup allows the simultaneous acquisition of mass spectrometric cyclic voltammograms (MSCVs) for selected masses and conventional voltammograms (CVs) recorded at a scan rate of 0.005 V s^{-1}. The anodic stripping of CO adsorbed at the different nanoparticles was studied after bubbling the gas for 10 min while polarizing the electrode at 0.07 V, replacing CO by Ar bubbling, and a subsequent potential scan up to 0.80 V in the base electrolyte solution at 25 °C. The upper potential limit was established at 0.80 V in order to prevent dissolution of Ru and Mo from the catalyst. Oxidation of the adlayer was followed by the mass signal for production of CO_2 ($m/z = 44$ corresponding to $[CO_2]^+$). Details of the procedure and electrochemical setup have been given elsewhere.[57,58]

Fourier transform infrared spectroscopy in situ (FTIRS) studies were performed with a Bruker Vector 22 spectrometer equipped with a MCT detector. A small glass cell with a 60° CaF_2 prism at its bottom was used. The cell and experimental arrangements have been described in detail elsewhere.[59,60] FTIR spectra were acquired from the average of 128 scans, obtained with 8 cm^{-1} resolution at selected potential, by applying single-potential steps from a reference potential (E_0) in the positive direction up to 0.80 V. The reflectance ratio R/R_0 was calculated, where R and R_0 are the reflectances measured at the sample and the reference potential, respectively. Accordingly, positive and negative bands represent the loss and gain of species at the sampling potential. P-polarized light was used for these experiments. Electrochemical control was carried out using a HEKA potentiostat-galvanostast PG310. For the study of CO oxidation to CO_2 in the presence of dissolved CO at 25 °C, the potential was set at $E = 0.05$ V in a CO-saturated electrolyte solution. A reference spectrum R_0 was run at 0.05 V, and then sample spectra R were measured every 0.05 V up to 0.80 V.

Chronoamperometric measurements in methanol solution were carried out at 25 and 60 °C. The electronic equipment consisted of a Radiometer Analytical model PGZ 301 potentiostat. The electrocatalytic activity of catalysts for methanol oxidation was studied in a 0.5 M H_2SO_4 and 2 M CH_3OH solution, where the potential was step from 0.10 to 0.60 V vs RHE.

Results and Discussion

Metal Nanoparticles Characterization. Analytical results of PtRu−MoO_x samples using TXRF, ICP, and TG techniques are compiled in Table 1. The combination of both TXRF and TG were necessary for calculation of metal loading of Pt, Ru, and Mo (wt %) since no reliable analysis of Ru was obtained by ICP. TXRF can only estimate the atomic ratio of Pt/Ru/Mo, while TG can be used to calculate the total amount of Pt^0 + RuO_2 + MoO_3, since XRD revealed that Pt, RuO_2, and MoO_3 are the only phases detected after sample firing in air. Values obtained by TG upon removal of the carbon substrate by air calcination at 600 °C are also reported in Table 1. Comparison of the Mo (wt %) obtained by two different techniques (ICP and TG) confirms the reliability of the analysis. It is seen that molybdenum values of MoO_x/C(1), MoO_x/C(2), and MoO_x/C(3) samples obtained by TG and ICP are comparable, and they are somewhat lower than nominal ones. However, incorporation of Pt and Ru by colloidal methodology decreases metal loading in all samples, mainly Mo, which are lost along the filtration step. For Mo-loaded samples, there is a strong dependence of Mo lost on the pH of the solution and more specifically in MoO_x/C(3). It is also observed that Mo loss is still higher in the MoO_x/C(2) sample prepared in the presence of H_2O_2. It is known that different Mo^{6+} species are developed depending on the pH of the solution: $MoO_2(H_2O)_4^{2+}$ (pH = 0), $MoO_3 \cdot xH_2O$ (pH = 2), polyanions $Mo_2O_7^{2-}$ and $Mo_7O_{24}^{6-}$ (pH = 2−7), MoO_4^{2-} (pH > 7), all of them, except hydrated MoO_3, being water soluble.[61] Taking this into account, it can be inferred that Mo is solubilized as polyanions during the synthesis of PtRu−MoO_x/C to ca. pH = 5 in aqueous solution.

(56) Schmidt, T. J.; Noeske, M.; Gasteiger, H. A.; Behm, R. J.; Britz, P.; Bönnemann, H. *J. Electrochem. Soc.* **1998**, *145*, 925.
(57) Planes, G. A.; García, G.; Pastor, E. *Electrochem. Commun.* **2007**, *9*, 839.
(58) Rodriguez, J. L.; Pastor, E.; Schmidt, V. M. *J. Phys. Chem. B* **1997**, *101*, 4565.
(59) Iwasita, T.; Nart, F. C. *VCH* **1995**, 123.
(60) Iwasita, T.; Nart, F. C. *Prog. Surf. Sci.* **1997**, *55*, 271.
(61) Holleman, A. F.; Wiberg, E. *Inorganic Chemistry*; Academic Press: New York, 2001; p 1382.

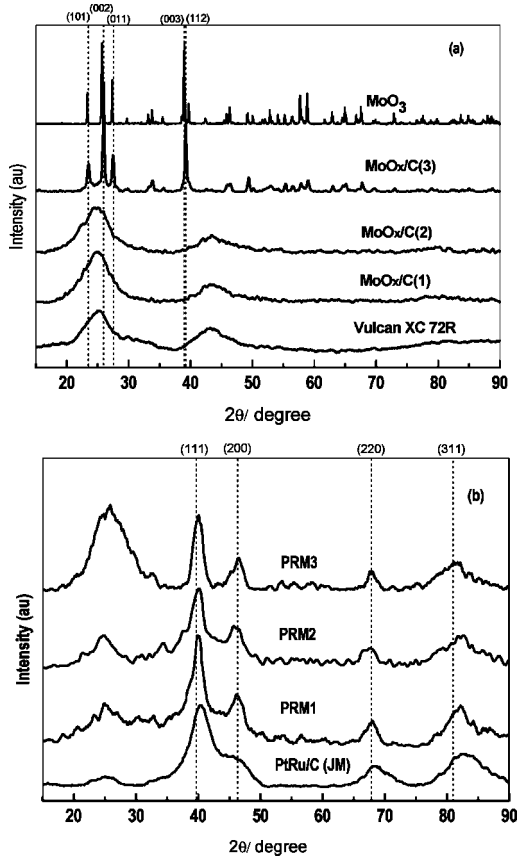

Figure 1. X-ray diffraction patterns of MoO_x/C samples (a) and ternary systems (b).

X-ray diffraction patterns of samples are shown in Figure 1. The Vulcan XC 72R substrate shows the characteristic diffraction pattern of graphitic carbon (Figure 1a). MoO_x/C(3) presents diffraction peaks typical of crystalline MoO_3 (JPCDS 47-1320). The diffraction lines observed at 2θ = 23.6°, 25.8°, 27.4°, 39.2°, and 39.3° are assigned to d(101), d(002), d(011), d(003), and d(112) diffraction of the MoO_3 phase (Figure 1a). The absence of these diffraction peaks in MoO_x/C(1) and MoO_x/C(2) could indicate that molybdenum species do not form crystalline aggregate, keeping a good dispersion. XRD patterns of the PRM samples in Figure 1b show the characteristic diffraction lines of Pt^0 metal (JPCDS 04-0802) with a low degree of crystallinity and the absence of crystalline platinum oxides. There is no shift to higher 2θ values with respect to the reflections of the Pt fcc structure.[62] At first glance, this result could suggest that Pt might constitute a nonalloyed phase with ruthenium, as opposed to what usually happens for supported PtRu catalysts (e.g., PtRu/C (JM)). Moreover, peaks of neither separate tetragonal RuO_2 nor hexagonal close-packed (hpc) Ru phases are found. However, PRM3 shows a broad peak between 20° and 30° and a peak at 39° which corresponds to crystalline MoO_3.

In order to asses the particle size of the metallic clusters on the carbon support, the (220) reflection of the Pt fcc structure was analyzed in detail. This reflection was selected because it appears in a diffraction range where the carbon substrate makes no contribution.[63] The average particle size was estimated from XRD patterns according to the Debye−Sherrer formula[64] and also from TEM images and histograms (Figure 2). The particle sizes estimated by these procedures (Table 1) are in good agreement, indicating that a homogeneous particle size distribution has been obtained, and they are on the order of 3−4 nm for PRM1 and PRM2, which are somewhat larger than the 2−3 nm for PRM3 and the commercial sample. In general, there is a good dispersion with some agglomeration of small particles.

Photoelectron spectroscopy analysis was used in order to obtain further information on the catalysts surface including the oxidation state of the elements. This information must be interpreted taking into account its limitations since the catalysts oxidation state probably changes during the electrochemical process. Both the substrate and PRM samples present three C 1s signals corresponding to graphitic carbon (284.4 eV), oxidized C−O (285.6 eV), and COO species (288.5 eV)[65,66] (see Table 1S in the Supporting Information). The S 2p signal of PRM samples displays two components, one small at 164.0 eV ($-S^*SO_3^-$ from $Na_2S_2O_5$) and one more intense at 168.4 eV ($-SS^*O_3^-$ from $Na_2S_2O_5$ or SO_3H^- from $HNaSO_3$).[67] Three components were fitted in the O 1s region. The peak at the lowest BE (530.0 eV) belongs to oxygen in metal oxide (Mo, Ru, and Pt) species.[66] The BE signal at ca. 531.0 eV suggests the presence of −C=O groups, and the signal at ca. 532.4−532.8 eV is attributed to higher oxidized groups on the carbon surface. Treatment with H_2O_2 in MoO_x/C(2) increases the concentration of these higher oxidized groups, also observed in PRM2 sample.[68,69]

The Mo 3d spectra for MoO_x/C(1), MoO_x/C(2), and MoO_x/C(3) in Figure 3 indicate the presence of Mo(VI) in hydrated $MoO_3 \cdot H_2O$ at ca. 233.5 eV and mainly Mo(VI) in MoO_3 species at ca. 232.5 eV.[66] Incorporation of Pt and Ru metals over MoO_x/C(1) and MoO_x/C(2) samples shifts the BEs of Mo 3d to lower values (ca. 233.1 and 231.9 eV, respectively), corresponding to a slightly reduction in MoO_x species. However, incorporation of Pt and Ru over MoO_x/C(3) shifts the BE of $MoO_3 \cdot H_2O$ to a higher value (234.0 eV), while the BE peak corresponding to MoO_3 at 232.3 eV does not change. The Pt 4f signal doublets in PRM samples are derived from two pairs of Pt species in similar concentrations (see Figure 1S in the Supporting Information). The Pt $4f_{7/2}$ component at ca. 72.2 eV is attributed to metallic Pt^0 particles interacting with the support. The component at ca. 74.5 eV corresponds to oxidized PtO species.[66] The reference JM has other components at 71.7 eV attributed to free Pt^0. The Ru $3p_{3/2}$ signal of PRM samples derives from two species with BEs of ca. 463.5 (RuO_2) and 466.3 eV (RuO_3) (see Figure 1S

(62) Chu, D.; Gilman, S. *J. Electrochem. Soc.* **1996**, *143*, 1685.
(63) Radmilovic, V.; Gasteiger, H. A.; Ross, P. N. *J. Catal.* **1995**, *154*, 98.
(64) *X-Ray Diffraction*; Addison-Wesley: Reading, MA, 1969.
(65) Boehm, H. P. *Carbon* **1994**, *32*, 759.
(66) Briggs, D.; Seah, M. P. In *Practical Surface Analysis by Auger and X-ray Photoelectron Spectroscopy*; Chichester, 1990.
(67) Cano-Serrano, E.; Campos-Martin, J. M.; Fierro, J. L. G. *Chem. Commun.* **2003**, 246.
(68) de la Fuente, J. L. G.; Martínez-Huerta, M. V.; Rojas, S.; Terreros, P.; Fierro, J. L. G.; Peña, M. A. *Carbon* **2005**, *43*, 3002.
(69) de la Fuente, J. L. G.; Rojas, S.; Martínez-Huerta, M. V.; Terreros, P.; Peña, M. A.; Fierro, J. L. G. *Carbon* **2006**, *44*, 1919.

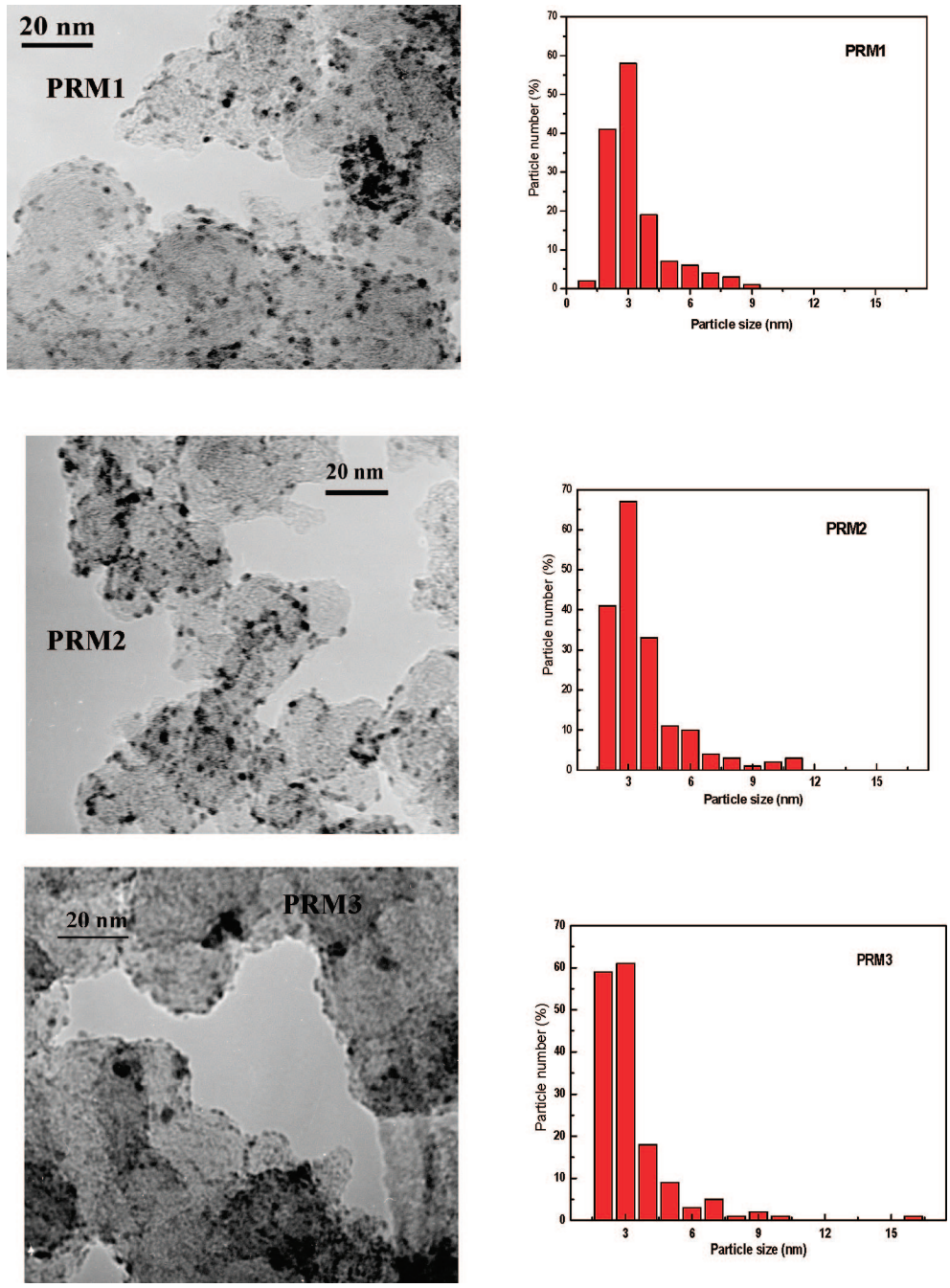

Figure 2. TEM images and the corresponding histograms for the PRM ternary systems (magnification 300k).

in the Supporting Information).[66] Nevertheless, the width of ca. 3 eV of these peaks suggests the presence of other phases with similar BE, like RuO_x.[70] The Ru $3p_{3/2}$ signal of JM sample shifts to lower BEs than ternary ones, indicating that ruthenium oxide species are present in a lower oxidation state (i.e., Ru(III)).

On the other hand, XPS indicates Mo oxide, Pt oxide, and Ru oxide species on the surface of the nanoparticles that can not be detected in the corresponding XRD pattern due likely to the very low thickness of the oxide layer (a few atomic layers) grown on top of the metal clusters. The calculated XPS surface concentrations of Pt and Ru are quite similar for the three PRM samples with a decrease of ca. 5 wt % in the Pt value compared to JM reference. Surface Mo loading decreases in PRM1 and PRM2 with respect to MoO_x/C(1) and MoO_x/C(2), respectively, but increases in PRM3 with respect to MoO_x/C(3). The substantial increase in Mo surface exposure in PRM3 regarding its parent noble-metal-free MoO_x/C(3) counterpart could indicate that molybdenum oxide is redispersed throughout incorporation of Pt and Ru, increasing its content at the surface.

The nature of the molybdenum species can be revealed by analyzing the reducibility behavior of carbon-supported MoO_x and PtRu—MoO_x electrocatalysts via temperature-programmed reduction (TPR) (Figure 4). The pure MoO_3 profile shows a broad peak with different shoulders at 714,

(70) Goodenough, J. B.; Manoharan, R.; Shukla, A.; Ramesh, K. V. *Chem. Mater.* **1989**, *1*, 391.

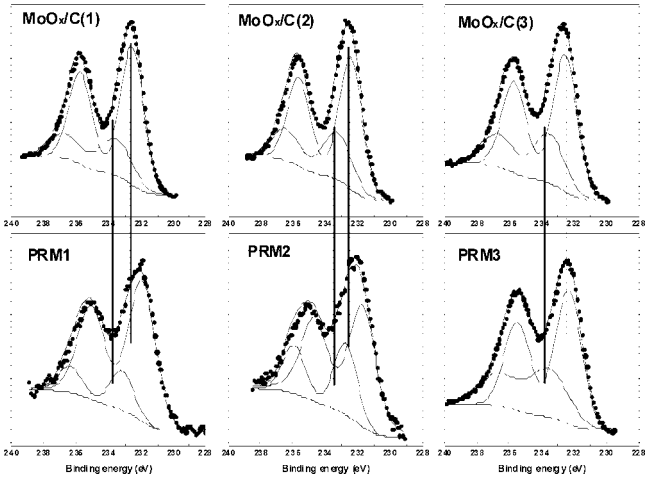

Figure 3. Mo3d core-level spectra of carbon-supported MoO_x/C and ternary PRM samples.

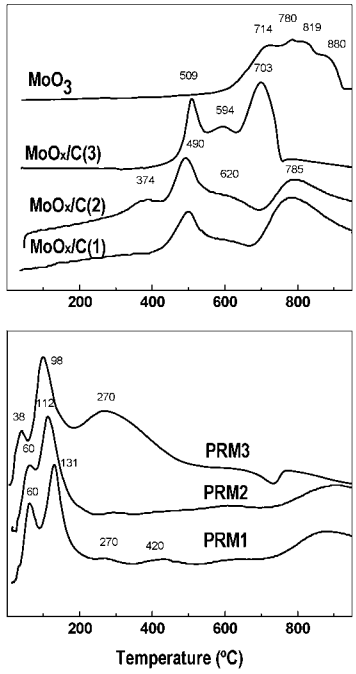

Figure 4. TPR profiles for MoO_x/C and ternary PRM samples.

780, 819, and 880 °C, which correspond to reduction of MoO_3 in various steps:[47,71] $MoO_3 \rightarrow MoO_2 \rightarrow Mo$. Reduction of MoO_3 to MoO_2 takes place in three different temperature regions, while reduction of MoO_2 to Mo metal takes place in one band. Although several MoO_x suboxides can be formed, they are not completely assigned. TPR spectra for MoO_x/C samples show similar profiles for MoO_x/C(1) and MoO_x/C(2). Both samples present three peaks at temperatures around 490, 620, and 785 °C and one more peak at 374 °C in MoO_x/C(2). A different TPR profile is observed in MoO_x/C(3), which records three peaks at 509, 594, and 703 °C. Though MoO_x/C(3) show similar diffraction lines to MoO_3 (Figure 1a), large differences can be observed in their TPR profile. These TPR differences between MoO_3 and MoO_x/C(3) are due to the fact that the reducibility of supported molybdenum oxide can be altered by the degree

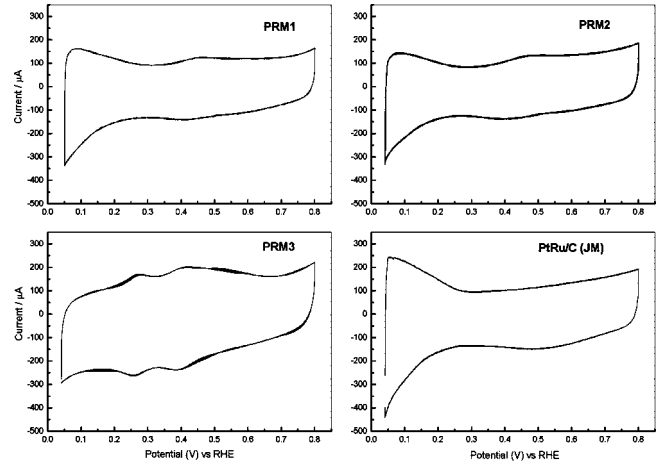

Figure 5. CV of the PRM1, PRM2, PRM3, and PtRu/C (JM) in 0.5 M H_2SO_4 at 25 °C.

of Mo−support chemical interaction and the nature of the surface species formed during sample MoO_x/C(3) preparation.

Higher temperature peaks at 785 °C in MoO_x/C(1) and MoO_x/C(2) and at 703 °C in MoO_x/C(3) are therefore assigned to reduction of MoO_2 with tetrahedral coordination to Mo^0, and lower temperature peaks are explained by reduction of different MoO_x suboxides with octahedral coordination formed during preparation.[72] Incorporation of Pt and Ru shifts molybdenum oxide peaks at lower temperatures. In general, TPR peaks between 30 and 60 °C are due to partially oxidized platinum, and reduction peaks between 98 and 131 °C correspond to a RuO_xH_y species.[73] The other peaks in PRM1, PRM2, and PRM3 are assigned to molybdenum oxide species.

Thus, incorporation of Pt and Ru by the colloidal method can substantially change the coordination of molybdenum oxide to obtain mainly Mo with octahedral coordination, although the precise molybdenum oxide phases have not yet been established. While PRM3 shows MoO_3 crystalline by XRD, this phase could not be inferred from its TPR profiles. In this way, the ability of Pt metal particles to enhance reduction of metal oxides by hydrogen via spillover processes[44,45,74] can be considered.

Cyclic Voltammograms and CO Adsorption Studies. In order to obtain further information on the chemical species of the electrocatalysts surface, cyclic voltammograms of the PRM1, PRM2, PRM3, and PtRu/C (JM) catalysts in 0.5 M H_2SO_4 at 25 °C were carried out and are shown in Figure 5. PtRu/C (JM) shows a characteristic cyclic voltammogram of PtRu catalysts without any peak in the 0.25−0.8 V region. On the contrary, PRM1 and PRM2 catalysts show one peak at ca. 0.44 V on a positive going scan, and another peak is visible on the negative-going scan at ca. 0.4 V. The cyclic voltammogram of PRM3 shows two peaks at ca. 0.27 and 0.4 V on a positive-going scan and its negative-going scan counterparts at 0.25 and 0.38 V. Earlier studies on PtMo/C

(71) Arnoldy, P.; de Jonge, J. C. M.; Moulijn, J. A. *J. Phys. Chem.* **1985**, *89*, 4517.
(72) Arnoldy, P.; Franken, M. C.; Scheffer, B.; Moulijn, J. A. *J. Catal.* **1985**, *96*, 381.
(73) Gómez de la Fuente, J. L. Ph.D. Dissertation, Universidad Autónoma de Madrid, 2007.
(74) Bond, G. C.; Tripathi, J. B. P. *J. Chem. Soc., Faraday Trans. I* **1976**, *72*, 933.

electrodes[41,24] show that the cyclic voltammograms of these catalysts are complex, and in most of cases only a tentative ascription of the peaks is possible, allowing a qualitative distinction between the reduction−oxidation response of Pt and that of Mo. From the comparison of the electrochemical response of pure Mo to that of PtMo alloy combined with an ex situ XPS study of the surface species of PtMo alloy, it has been suggested that Mo is present in the oxidized form in the entire potential window, changing from Mo^{3+} to Mo^{6+} as the potential increases.[40,41] Recently, in in situ XAS studies of the surface species of PtMo/C catalysts,[75] the Mo K edge XANES spectra at 0.0 V shows that Mo is present as a hydrated oxide species with an approximated oxidation state of Mo^{5+}, and there is a change in the oxidation state of Mo from Mo^{5+} to Mo^{6+} at 0.54 V, which remains the same at 0.85 V. In our voltammetric results the redox couple observed in PRM1 and PRM2 catalysts at ca. 0.45 V do agree with the presence of Mo in an oxidation state between Mo^{5+} and Mo^{6+}. Ex situ XPS confirms the presence of MoO_x species, whose binding energy is slightly lower than the Mo^{6+} species. Therefore, the redox couple in PRM1 of PRM2 can be attributed to the reduction/oxidation of Mo^{5+}/Mo^{6+} to intermediate MoO_x ($2.5 < x < 3$) oxides in acidic solution. Although some authors emphasized the relevance of the hydrogen molybdenum bronze for this reaction, studies carried out by Endres et al.[76] found that hydrogen molybdenum bronzes (H_xMoO_3) are partly solubilized in 0.5 M H_2SO_4. No peak associated with formation of H_xMoO_3 species has been found in PRM1 and PRM2 catalysts. In addition, the electrochemical surface of both catalysts remains stable under acidic conditions. These two facts preclude hydrogen molybdenum bronze as being responsible for the CO tolerance. In PRM3, the oxidation peaks correspond to different MoO_x species with different oxidation states between Mo^{5+} and Mo^{6+}. In this case a gradual decrease of the peaks, related to the reduction−oxidation reactions of Mo, was evident after 50 cycles of the working electrode, suggesting that Mo dissolved into the electrolyte.

The electrooxidation of CO adsorbed on electrocatalysts (stripping technique) provides information about the facility of the material for CO oxidation, and the extent of this process gives information about the active surface area accessible to the reactants, intrinsic catalytic activity, and, in some cases, catalyst surface composition. A low onset potential of CO oxidation indicates a good CO tolerance of the electrocatalyst. However, exact determination of the onset for CO_2 from the electrochemical current includes certain difficulties given the need for double-layer correction and sometimes the presence of other faradaic corrections. In this case, differential electrochemical mass spectrometry (DEMS) or in situ infrared spectroscopy (FTIRS) are more appropriate since no faradaic or double-layer corrections are needed.

The CVs and simultaneously recorded MSCVs related to production of CO_2 ($m/z = 44$, corresponding to the radical cation $[CO_2]^{\bullet+}$) (DEMS analysis) during the electrooxidation of CO adsorbed on the electrocatalysts at 60 °C are given in Figure 6. The curves confirm the cell setup allowed for online detection of the faradaic current and CO_2 production. Peak potentials (E_{peak}) for the mass signal $m/z = 44$ recorded during the first positive potential scan after adsorption as well as the onset potentials (E_{onset}) for CO_2 production are given in Table 2. PRM1 and PRM2 samples show the onset for CO_2 production at 60 °C at 0.12 V, which represents a negative shift of 0.20 V with respect to PtRu/C (JM) at the same temperature. On the other hand, E_{peak} appears at about 0.10 V shifted to more negative potentials in PtRu/C (JM) than in PRM1 and PRM2 samples. This could indicate that different Pt−Ru interactions take place in the phases for PRM1 and PRM2, compared with PtRu/C (JM) materials. It is remarkable that even though the peak potential is more appropriate for the JM catalysts, the fact that CO can be oxidized at more negative potentials for PMR1 and PMR2 is of great interest because this implies that oxidation of this catalytic poison occurs easily at the potentials of operation in a PEMFC and DMFC.

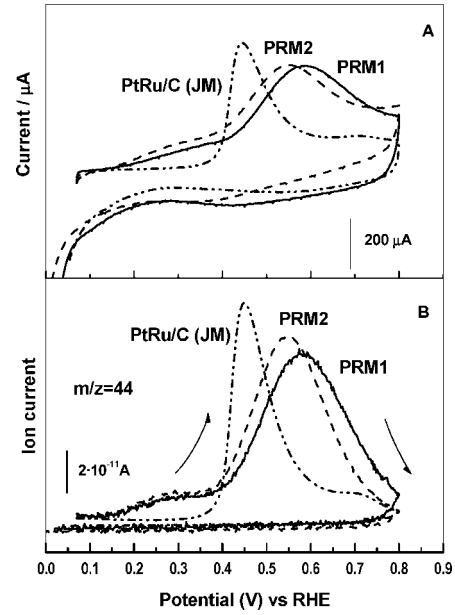

Figure 6. CV for the oxidation of adsorbed CO in 0.5 M H_2SO_4 at 60 °C (A) of PRM1, PRM2, and PtRu/C (JM) and the corresponding signal for CO_2 production ($m/z = 44$) (B), $\upsilon = 0.005$ V s^{-1}. Catalyst loading: 0.12 mg for PRM1 and PRM2 and 0.08 mg for PtRu/C (JM).

Table 2. Potentials for Maximum Ion Current (E_{peak}) and Onset (E_{onset}) for the Mass Signal $m/z = 44$ during the First Electro-Oxidation Cycle After CO Adsorption at 0.07 V

	25 °C		60 °C	
sample	E_{onset} (V)	E_{peak} (V)	E_{onset} (V)	E_{peak} (V)
PRM1	0.16	0.66	0.12	0.57
PRM2	0.13	0.66	0.12	0.54
PRM3	0.30	0.58		
PtRu/C (JM)	0.34	0.57	0.32	0.45

The same experiments were repeated at 25 °C (thus the behavior at room temperature is evaluated, which is of interest for DMFC applications), and significant potentials are reported in Table 2. As expected, it is observed that for PMR1 and PMR2 adsorbed CO can be easily oxidized at 60 °C and a potential shift of about 0.10 V to more positive potentials for E_{peak} is established at 25 °C. On the other hand, almost no shift is recorded for E_{onset}. These results are entirely

(75) Mukerjee, S.; Urian, R. C. *Electrochim. Acta* **2002**, *47*, 3219.
(76) Endres, F.; Schwitzgebel, G. *J. Electroanal. Chem.* **1996**, *415*, 23.

reproducible, and the CVs remain stable during potential cycling and after CO stripping. However, a more detailed inspection of the MSCVs at both temperatures shows that the contribution to the CO_2 signal in the 0.10−0.30 V potential range is increased for PRM1 and PRM2 samples at 60 °C with respect to 25 °C, as expected.

The PRM3 catalyst displays a different behavior (not shown). Although PRM3 presents the highest Mo loading, its CO electrooxidation behavior is similar to that of PtRu/C (JM) catalysts. Thus, the maximum in the ion current in both materials is achieved at ca. 0.57 V (see Table 2) and the contribution to the CO_2 signal in the 0.10−0.30 V observed for PRM1 and PRM2 is not apparent in this case. The onset for CO_2 at PRM3 only shifts 0.06 V to negative values with respect to the commercial catalyst, and some dissolution of Mo in the electrolyte was detected.

Cyclic voltammograms of PRM1, PRM2, and PtRu/C (JM) after CO electrooxidation are identical in voltammograms before CO adsorption studies (not shown). However, PRM3 shows a large decrease of the peaks due to dissolution of Mo in the electrolyte.

The FTIRS technique was used for studying CO electrooxidation in the presence of dissolved CO to envisage the technological use of these materials as anode electrodes in PEMFC fed with H_2 produced by steam reforming of hydrocarbons or alcohols (and therefore containing traces of CO). These experiments cannot be performed with DEMS, as the system is continuously evacuated and, accordingly, the CO from the solution is continuously pumped into the vacuum system and its concentration decreases avoiding saturation. Series of spectra obtained at different potentials with p-polarized light in the presence of CO in the electrolyte solution, at room temperature, are given in Figure 7. p-Polarized light is sensitive to both solution and surface species. Thus, the negative bands at ca. 2343 cm^{-1} for all samples in these curves correspond to formation of CO_2 in the solution. On the other hand, the positive features in the 2040−2050 cm^{-1} region are assigned to adsorbed terminal-bonded CO. Electrooxidation of adsorbed CO in the presence of the dissolved gas can then be followed by the evolution of these bands with the potential. For the sake of comparison, spectra have been normalized by the CO_2 signal recorded at 0.80 V.

FTIR spectra for PRM1 and PRM2 show the onset for CO_2 formation (band at 2343 cm^{-1}) at 0.25 and 0.20 V, respectively. A positive shift of 0.1 V in E_{onset} is established from the comparison with experiments in the absence of dissolved CO. The reference sample (JM) shows similar behavior. This shift is typical for experiments in the presence of CO in the solution.[77,78] However, it is noteworthy that in these conditions the onset for CO_2 for PRM2 is still more negative than for PtRu/C (JM).

The ratio of the intensities of the infrared bands associated to terminal-bonded CO and CO_2 is lower in Mo-containing samples (1.03 for PRM1 and 0.12 for PRM2 at 0.8 V) compared with PtRu/C (JM) (3.07 at 0.8 V). This suggests that lower amounts of CO are adsorbed, and therefore, the surface is less poisoned, allowing production of higher amounts of CO_2 from dissolved CO. This fact is especially remarkable for the samples treated with H_2O_2 (PRM2). Consequently, the presence of MoO_x and a more oxidized surface of the carbon support go some way to avoiding the bonding of CO to PtRu.

Methanol Electrooxidation. Electrochemical oxidation of methanol on a PtRuMo/PANI catalyst has been reported to take place 0.1 and 0.2 V shifted to more negative potentials with respect to PtRu/PANI and Pt/PANI, respectively.[29,30] According to these results, although the support is different in our case, it is expected that our carbon-supported catalysts also have higher performances for the oxidation of methanol than the PtRu/C (JM).

Regarding technical applications, it is desirable for activating effects to be sustained over long periods of time. Therefore, the results from basic experiments designed to judge and compare the capability of electrocatalysts for methanol electrooxidation are usually obtained in the form of current−time curves at constant potential normalized for the area estimated from CO_{ads} stripping voltammograms.[75] As the amount of CO_{ad} is directly related to the amount of the bi/trimetallic alloy nanoparticles, the charge involved in the process reflects the real electrochemical area of the electrode.[76,77,79] Figure 8 shows current−time curves for PRM1, PRM2, PRM3, and PtRu/C (JM) toward methanol oxidation at 25 (A) and 60 °C (B). The applied potential for these experiments has to be selected next to the potential in a DMFC but also where a significant oxidation current density is recorded (at 0.50−0.55 V, the current for all these electrodes is very low, see Figure 2S in the Supporting Information). A working potential of 0.60 V was used; this potential is more positive than the approximately 0.50 V of the DMFC, but it has to be considered that the three-electrode configuration employed in the present experiments is not completely equivalent with the two-electrode configuration in the DMFC.

The chronoamperometric curves shown in Figure 8 correspond to a potential step from 0.10 to 0.60 V, and the state of the surface at the initial potential is different at 25 and 60 °C. At 25 °C, the surface is free from adsorbates (almost no adsorption occurs at 0.10 V) and the step to 0.60 V produces a high initial current. At this potential, methanol starts to be oxidized at a "clean" surface. With time, the current decreases because of the partial poisoning of the catalysts (the potential is not positive enough to completely oxidize the intermediates) and methanol consumption. At 60 °C, catalysts adsorb methanol at 0.10 V (see Figure 3S in the Supporting Information) and during the first seconds of the step to 0.60 V oxidation of the adsorbates prevails, especially in PRM1 and PRM2. The surface is partially covered (in this case methanol does not react on a clean surface), and as the catalyst becomes "cleaner" the current increases. Finally, in both cases, an almost stationary current is achieved.

It was observed that ternary PRM1 and PRM2 catalysts perform better than PtRu/C (JM) and PRM3, especially at

(77) Wolter, O.; Heitbaum, J. *Ber. Bunsen-ges. Phys. Chem.* **1992**, *317*, 291.
(78) López Cudero, A. Ph.D. Dissertation, Universidad Autónoma de Madrid, 2005.
(79) Gasteiger, H. A.; Markovic, N. M.; Ross, P. N.; Cairns, E. J. *J. Phys. Chem.* **1994**, *98*, 617.

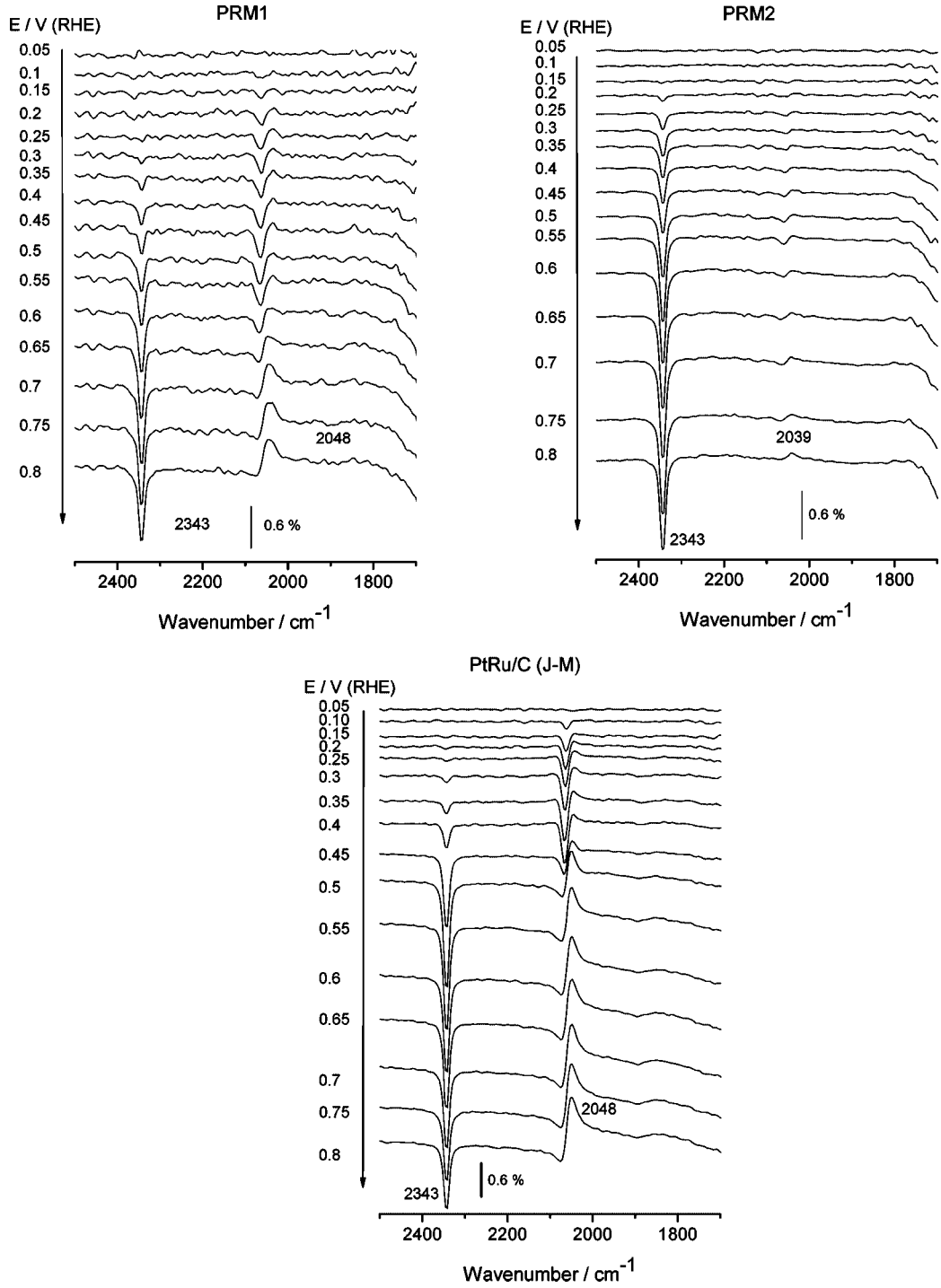

Figure 7. In situ FTIR spectra obtained in CO-saturated solution (base electrolyte = 0.5 M H_2SO_4). E_{ref} = 0.05 V, 128 scans, 8 cm^{-1}, p-polarized light.

60 °C. These results are particularly interesting as incorporation of a small amount of Mo significantly increases the intrinsic catalytic activity to methanol electrooxidation. PRM3 presents higher Mo loading but with a MoO_x phase, which is not active for methanol oxidation.

These results confirm those previously described above. It was established that the presence of small amounts of Mo increases CO tolerance. The same effect is also observed for methanol electrooxidation. It is known that an important, although not unique, aspect of the catalysis of methanol oxidation is related to catalysis of CO oxidation. The mechanism for direct MeOH oxidation has two possible rate-limiting steps: (i) initial abstraction of the C−H bond and adsorption of the methanolic species and (ii) eventual oxidation of CO species formed as intermediate after deprotonation of methanol during adsorption. It therefore seems that the increase in the performance of methanol oxidation in PRM1 and PRM2 catalysts is based on their less CO-poisoned surface, according to the FTIR results.

On the basis of the physicochemical and electrochemical characterization of the catalysts, incorporation of Pt and Ru metals on a carbon substrate (MoO_x/C) following a colloidal method developed by Watanabe at al. yields MoO_x, RuO_xH_y, and Pt^0 species with particle size in the nanoscale range (3−4

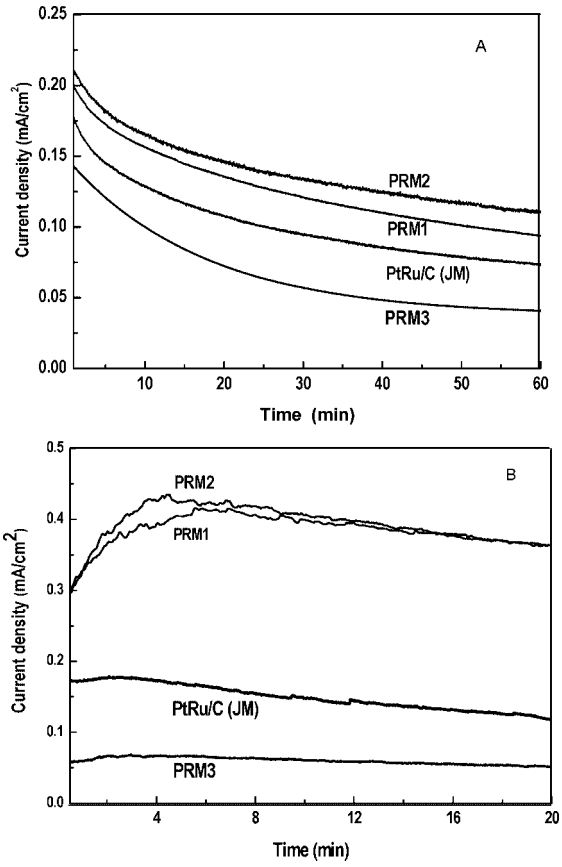

Figure 8. Electrocatalytic activities at 0.60 V in terms of current−time dependence for PRM1, PRM2, and PtRu (JM) electrocatalysts toward methanol oxidation at (A) 25 and (B) 60 °C. Current scale is normalized for the area estimated from CO_{ads} stripping voltammograms.

nm). TPR profiles show that this incorporation can substantially change the coordination of molybdenum oxide, whereas the importance of the molybdenum precursor cannot be neglected. For instance, the precursor $MoCl_5$ provides dispersed PtRu metal on MoO_x ($2.5 < x < 3$)/carbon substrate in both PRM1 and PRM2. The most important criterion for estimating CO tolerance of electrocatalysts is the ignition potential at which CO adsorbed on the catalyst is oxidized and the current rises rapidly.[80] On the basis of DEMS measurements, it is evident that the onset potential to CO_2 starts at a lower potential on PRM1 and PRM2 than on PtRu/C (JM), indicating that the mechanism to CO electrooxidation has varied due to the interaction between noble metals and the MoO_x species. The CO oxidation process in the 0.10−0.30 V potential range for PRM1 and PRM2 catalysts suggests that good proximity and mixing of the molybdenum oxide species, whose oxidation state would be between Mo^{5+} and Mo^{6+}, on the surface of carbon substrate along with mixed PtRu nanoparticles is essential for the tolerance mechanism. Also, in situ FTIR studies in the presence of dissolved CO show that lower amounts of CO are adsorbed on PtRu−MoO_x catalysts than in binary catalyst, and this is particularly remarkable for the samples treated with H_2O_2 (PRM2). Therefore, it may be concluded that molybdenum could influence in the electrooxidation of CO in two different ways. First, MoO_x weakens the CO interaction with the surface, according to the ligand effect. Second, MoO_x provides new active sites for electrooxidation of CO at potentials below 0.3 V, which may enhance the availability of reactive oxygen at the surface, according to a bifunctional mechanism. Nevertheless, further investigations are required in order to understand the interactions between MoO_x and PtRu nanoparticles.

(80) Grgur, B. N.; Markovic, N. M.; Ross, P. N. *Electrochim. Acta* **1998**, *43*, 3631.

5. Conclusions

Significantly CO-tolerant carbon-supported PtRu−MoO_x nanoparticles with smaller amounts of noble metals Pt and Ru than commercial ones were prepared following a new two-step procedure. In the first step, carbon-supported molybdenum oxides (MoO_x/C) were prepared by impregnation with a $MoCl_5$ precursor to obtain MoO_x/C(1) and MoO_x/C(2) (treated with H_2O_2). In the second step, Pt and Ru were incorporated following a colloidal method with $NaHSO_3$ to obtain PRM1 and PRM2 samples. These materials show mainly MoO_x, RuO_xH_y, and Pt^0 species on the black carbon substrate. Oxidation with aqueous H_2O_2 during the preparation of MoO_x/C(2) mainly affects the atomic ratio of Pt/Mo (PRM2) and increases the oxidized surface with no influence on the sample nanostructure. The particle size of the metal active phase of these materials was found to be in the nanoscale range (3−4 nm) with some agglomeration of small particles.

PRM1 and PRM2 show a significant increase of CO tolerance in comparison with commercial (JM) sample. From differential electrochemical mass spectrometry, a significantly negative shift of about 0.2 V in the onset potential for CO_2 was established for these systems with respect to commercial PtRu/C (JM) at room temperature and 60 °C. Moreover, an increase in CO_2 production for $E < 0.40$ V is observed at 60 °C for both PRM1 and PRM2. In situ FTIR spectra acquired in CO-saturated solution suggest that the metal surface is less poisoned with CO, especially when a H_2O_2 solution is used to obtain PRM2. Furthermore, the activity toward methanol oxidation is higher, especially at 60 °C, for PRM1 and PRM2 than for PtRu/C (JM). The results of this work are highly encouraging as it is proved that a reduction in the amount of precious metals is possible in parallel with a significant increase in CO tolerance in comparison with commercial catalysts.

Acknowledgment. This research was funded by the Ministry of Education and Science, Spain (Projects ENE2004-07345-C03-01/ALT and MAT2005-06669-C03-02). M.V.M.H. acknowledges the Juan de la Cierva program of the Ministry of Science and Technology of Spain for its financial support. N.T. acknowledges the I3P program (CSIC) for financial support.

Supporting Information Available: Binding energies (eV) of core levels of electrocatalysts (Table S1), Pt4f and Ru3p core-level spectra of electrocatalysts (Figure S1), CV for the oxidation of methanol in 0.5 M H_2SO_4 + 2 M CH_3OH at 25 °C of PRM1, PRM2, and PtRu/C (JM) $\upsilon = 0.02$ V s^{-1}, whose current scale is normalized for the area estimated from CO_{ads} stripping voltammograms (Figure S2), and CV for the oxidation of methanol in 0.5 V H_2SO_4 at 58 °C of PtRu/C catalyst (Figure S3) (PDF). This material is available free of charge via the Internet at http://pubs.acs.org.

CM703047P